Water Resources Research

RESEARCH ARTICLE
10.1029/2018WR022981

Evaluating Soil Resistance Formulations in Thermal-Based Two-Source Energy Balance (TSEB) Model: Implications for Heterogeneous Semiarid and Arid Regions

Yan Li[1,2,3], William P. Kustas[2], Chunlin Huang[1], Hector Nieto[4], Erfan Haghighi[5,6], Martha C. Anderson[2], Francisco Domingo[7], Monica Garcia[8,9], and Russell L. Scott[10]

[1]Key Laboratory of Remote Sensing of Gansu Province, Heihe Remote Sensing Experimental Research Station, Cold and Arid Regions Environmental and Engineering Research Institute, Chinese Academy of Sciences, Lanzhou, China, [2]U.S. Department of Agriculture, Agricultural Research Service, Hydrology and Remote Sensing Lab, Beltsville, MD, USA, [3]University of Chinese Academy of Sciences, Cold and Arid Regions Environmental & Engineering Research Institute, Beijing, China, [4]Edifici Fruitcentre, Efficient Use of Water in Agriculture program IRTA Parc de Gardeny, Lleida, Spain, [5]Department of Civil and Environmental Engineering, Massachusetts Institute of Technology, Cambridge, MA, USA, [6]Department of Water Resources and Drinking Water, Swiss Federal Institute of Aquatic Science and Technology, Dübendorf, Switzerland, [7]Estación Experimental de Zonas Áridas, Consejo Superior de Investigaciones Científicas (EEZA-CSIC), Almería, Spain, [8]Department of Environmental Engineering, Denmark Technical University (DTU), Kgs. Lyngby, Denmark, [9]International Research Institute for Climate and Society, The Earth Institute, Columbia University, Palisades, NY, USA, [10]U.S. Department of Agriculture, Agricultural Research Service, Southwest Watershed Research Center, Tucson, AZ, USA

Key Points:
- A new soil resistance formulation has been integrated into the two-source energy balance (TSEB) model
- The new soil resistance formulation has low sensitivity to uncertainty in model coefficients
- With the new soil resistance formulation implemented in TSEB, model output of sensible heat flux was in good agreement with measurements in heterogeneous semiarid and arid regions

Correspondence to:
W. P. Kustas,
bill.kustas@ars.usda.gov

Citation:
Li, Y., Kustas, W. P., Huang, C., Nieto, H., Haghighi, E., Anderson, M. C., et al (2019). Evaluating soil resistance formulations in thermal-based two-source energy balance (TSEB) model: Implications for heterogeneous semiarid and arid regions. *Water Resources Research*, *55*, 1059–1078. https://doi.org/10.1029/2018WR022981

Received 20 MAR 2018
Accepted 17 NOV 2018
Accepted article online 26 NOV 2018
Published online 7 FEB 2019

Abstract Relatively small fluctuations in the surface energy balance and evapotranspiration in semiarid and arid regions can be indicative of significant changes to ecosystem health. Therefore, it is imperative to have approaches for monitoring surface fluxes in these regions. The remote sensing-based two-source energy balance (TSEB) model is a suitable method for flux estimation over sparsely vegetated semiarid and arid landscapes since it explicitly considers surface energy flux contributions from soil and vegetation. However, previous studies indicate that TSEB generally underestimates sensible heat flux (*H*) and hence overestimates latent heat flux (*LE*) or evapotranspiration for these regions unless soil resistance coefficients are modified based on additional ground information. In this study, TSEB is applied over semiarid and arid regions on three continents using the original soil resistance formulation with modified coefficients and a recently developed physically based soil resistance formulation. Model sensitivity analysis demonstrates the high sensitivity of TSEB with original soil resistance formulation to soil resistance coefficients, while TSEB with the new soil resistance formulation has relatively low sensitivity to uncertainties in all coefficients. The performance of TSEB using different soil resistance formulations is evaluated by comparing modeled *H* against eddy covariance measurements in six semiarid and arid study sites and ranking the error statistics. Our results indicate that incorporating the new soil resistance formulation into TSEB would enhance its utility in flux estimation over heterogeneous landscapes by obviating its reliance on semiempirical coefficients and thus provide more robust fluxes over sparsely vegetated regions without model calibration and/or parameter tuning.

1. Introduction

Semiarid and arid regions occupy approximately 25% of Earth's land surface. These regions are characterized by limited water resources, sparse vegetation, and fragile ecosystems (Fensholt et al., 2012). In these regions, more than 90% of annual rainfall returns to the atmosphere as evapotranspiration (ET; Garcia et al., 2013; Wilcox et al., 2003). Accurately estimating the spatial and temporal distribution of ET or the latent heat flux (*LE*) is critical for monitoring ecosystem health (Moran, 2004) and improving water resources management (Dinpashoh, 2006) in these regions. Remote sensing can provide estimates of ET over a wide range of temporal and spatial scales by providing spatially distributed surface information related to water and energy fluxes, which include land surface temperature, soil moisture, and vegetation cover (Huang et al., 2015). Over the last few decades, several methods have been proposed for estimating ET and surface fluxes based on remotely sensed data, which can be divided into four main categories (Li et al., 2017): (1) empirical and semiempirical approaches, (2) surface energy balance (SEB) models, (3) traditional ET approaches (i.e., the Penman-Monteith and Priestley-Taylor [PT] approaches) combined with remotely sensed data, and (4) data assimilation combined with land surface models and remote sensing observations.

This study focuses on SEB modeling, in which *LE* is calculated as the residual of available energy (i.e., the difference between net radiation and soil heat flux) minus sensible heat flux (*H*), which is estimated via surface-to-air temperature gradient (Kustas & Anderson, 2009). SEB models can be classified into two main categories: single-source models that do not distinguish energy fluxes from soil and vegetation elements and two-source models that explicitly treat soil and vegetation canopy energy exchanges with the lower atmosphere (Kalma et al., 2008). Single-source modeling has been used to estimate ET and surface energy fluxes over a wide range of scales, climate conditions, and land cover types and has performed reasonably well, especially for irrigated cropland covered by dense vegetation (Elhag et al., 2011; Huang et al., 2015; Li et al., 2017; Van der Kwast et al., 2009). However, for sparsely vegetated surfaces in semiarid and arid regions, single-source models can produce large errors in surface energy fluxes (Cleugh et al., 2007). Flux estimates from single-source models can be improved with a prior calibration of resistance parameters based on in situ flux measurements (Gokmen et al., 2012; Huang et al., 2015; Kustas et al., 2016; Kustas & Anderson, 2009). However, the need to perform a calibration limits the utility of single-source models applied to sparsely vegetated complex landscapes located in semiarid and arid climates.

To accommodate the effects of partially vegetated surfaces on turbulent energy exchange and radiometric land surface temperature, Norman et al. (1995) proposed the thermal-based two-source energy balance (TSEB) model, which considers surface energy flux contributions from soil and vegetation using component temperatures from soil (T_s) and canopy (T_c) as well as the partitioning of radiation and heat fluxes between soil and canopy elements. The original TSEB formulation of Norman et al. (1995) provides two different resistance networks: a parallel approach and a series approach. Previous studies found that the series approach, which considers interaction between soil and canopy, is more robust (Morillas et al., 2013; Song et al., 2016). TSEB and its revisions (Anderson et al., 1997; Colaizzi et al., 2012; Kustas & Norman, 1999, 2000) have been successfully applied to compute surface energy fluxes and produced daily ET maps over a wide variety of fractional vegetation cover and soil moisture conditions based on remotely sensed data (Anderson et al., 2011). Moreover, TSEB is not only able to provide soil evaporation and canopy transpiration separately but also shown to be more robust than single-source models when applied to complex landscapes and more extreme climatic conditions (Kustas & Anderson, 2009; Tang et al., 2011; Timmermans et al., 2007; Zhan et al., 1996).

Nevertheless, the utility of TSEB in surface flux estimation over heterogeneous semiarid and arid regions is challenging since it is characterized by low ET due to low water availability (Garcia et al., 2013; Morillas et al., 2013). The original TSEB formulation tested by Norman et al. (1995) in semiarid desert gave good results. However, more recently, Morillas et al. (2013) showed that TSEB significantly underestimated *H* over semiarid Mediterranean tussock grassland, leading to large positive biases in *LE* computed as a residual by TSEB. A follow-up analysis by Kustas et al. (2016) suggested that key vegetation inputs and the semiempirical coefficients of the soil resistance formulation used in estimating sensible heat flux from the soil surface lead to a large bias in estimates of *H* over this semiarid grassland site. Reliable results for this site were achieved primarily by modifying the coefficients in the soil resistance formulation based on ground observations of the soil roughness and vegetation characteristics at the field site (Kustas et al., 2016). The soil resistance coefficients beneath a canopy can be determined with heat flux measurements at the soil surface, and temperature and vapor pressure profiles from soil surface to canopy air space (Sauer et al., 1995). Such detailed measurements are rare while ground-based information on soil roughness and vegetation distribution and architecture are not routinely available, so that refining the soil resistance coefficients may be difficult to implement operationally. The need for more robust model formulations to estimate soil surface fluxes has recently been highlighted by Talsma et al. (2018) as critical for improving remote sensing-based model estimates of ET partitioning between soil and vegetation.

Haghighi and Or (2015b) proposed a physically based model for simulating soil evaporative fluxes with a new soil resistance formulation for turbulent heat transport based on fundamental fluid dynamic principles and validated this scheme at the microscale using small laboratory wind tunnel data. The new soil resistance used in Haghighi and Or (2015b) is appropriate for drying soil surfaces covered by bluff-body obstacles and explicitly considers aerodynamic interactions between adjacent bluff bodies. This new scheme has been successfully applied to sparsely vegetated semiarid areas, providing theoretical estimates of turbulent heat fluxes and their partitioning (Haghighi & Kirchner, 2017). To reduce overestimates of *LE* in the community atmosphere biosphere land exchange land surface model, Decker et al. (2017) incorporated a previous version of this new soil resistance that explicitly accounts for subsurface viscous losses constraining soil

evaporation fluxes (Haghighi et al., 2013; Haghighi & Or, 2015a). Results of Decker et al. (2017)'s study showed that errors in daily H and LE tend to reduce when empirical formulations of soil resistance in community atmosphere biosphere land exchange are replaced by this physical-based formulation. Recently, this new physically based scheme and the original soil resistance formulation used in TSEB were compared over an irrigated vineyard (Li et al., 2018). The results indicated that the new scheme outperformed the original formulation using standard soil resistance coefficients and offered an opportunity to advance the utility of TSEB model when applied to sparsely vegetated areas. Given these promising findings, this new formulation has been incorporated in TSEB to enhance its utility in estimating fluxes over sparsely vegetated semiarid and arid regions where the ground-based observations are not typically available for modifying soil resistance coefficients and thus advance its operational capabilities by requiring minimal ground information.

The objective of this study is to assess the performance of TSEB with soil resistance formulation using typical coefficients (Kustas & Norman, 1999), modified coefficients for semiarid clumped vegetation with rocky soil surfaces (Kustas et al., 2016), and the new soil resistance formulation proposed by Haghighi and Or (2015b, 2015c, 2015d) over heterogeneous semiarid and arid regions. To reduce input errors in running TSEB, local ground-based vegetation parameters and radiometric land surface temperature during daytime conditions are used. Data used in this study are from six field sites with flux tower measurements under water-limited conditions in natural semiarid and arid regions. Since TSEB is a residual-based approach, we evaluate model performance based on H measurements from eddy covariance (EC) towers. In this way, we are not confounding model performance with errors in estimates of available energy and lack of energy balance closure with EC systems. In addition, a new model evaluation strategy proposed by Best et al. (2015) is used to evaluate model performance, which leads to less ambiguous conclusions based on the selected performance criteria and allows for an explicit framework for stepwise hypothesis testing. To identify the influencing parameters of TSEB over natural semiarid and arid regions, a global sensitivity analysis was conducted for evaluating the effects of key inputs and soil resistance coefficients to TSEB with original and the new soil resistance formulation.

2. Methodology

2.1. TSEB Model

The TSEB model, originally proposed by Norman et al. (1995) for estimating component surface energy fluxes from soil and vegetation using observations of directional radiometric temperature, was developed to accommodate a wider range of land cover and environmental conditions. Several revisions to TSEB algorithms have been subsequently implemented, which include improving estimates of net radiation for soil and vegetation based on a more physically algorithm proposed by Campbell and Norman (1998) and refining formulations for soil resistance terms (Kustas & Norman, 1999, 2000). There have also been proposed improvements to the soil and vegetation partitioning of temperatures and radiation for row crops (Colaizzi et al., 2012, 2014) as well as a transpiration algorithm based on Penman-Monteith canopy conductance instead of PT (Colaizzi et al., 2013, 2014). In this study, the original TSEB including refinements by Kustas and Norman (1999, 2000) was considered suitable for modeling the SEB of landscapes containing sparse randomly distributed clumped vegetation.

In TSEB, the surface energy budgets are separately balanced for soil and vegetation:

$$R_n = LE + H + G, \tag{1}$$

$$R_{nc} = H_c + LE_c, \tag{2}$$

$$R_{ns} = H_s + LE_s + G, \tag{3}$$

where R_n is net radiation, G is soil heat flux, H is sensible heat flux, and LE is latent heat flux (all in W/m^2). Subscripts s and c represent soil and vegetation scene components, respectively. All the composite surface fluxes for the combined soil-vegetation system in equation (1) can be estimated as the sum of soil and vegetation components except G, which is parameterized as a fraction of R_{ns},

$$G = c_G R_{ns}, \tag{4}$$

where c_G is an empirical coefficient, which is constant for several hours around solar noon (Kustas & Daughtry, 1990). Details of estimating R_{ns} and R_{nc} can be found in Kustas and Norman (1999) and Morillas et al. (2013). For incomplete vegetation cover, Colaizzi et al. (2016, 2016) proposed a soil heat flux model that calculate G as a function of shaded, partially sunlit, or fully sunlit R_{ns}.

By permitting the interaction between soil and vegetation, Norman et al. (1995) proposed a *series* soil-vegetation resistance network to estimate sensible heat flux (H), which is defined as

$$H = H_s + H_c = \rho C_P \frac{T_{ac} - T_a}{r_a}, \tag{5}$$

with

$$H_s = \rho C_P \frac{T_s - T_{ac}}{r_s}, \tag{6}$$

$$H_c = \rho C_P \frac{T_c - T_{ac}}{r_x}, \tag{7}$$

where H_s and H_c are sensible heat flux from soil and vegetation, respectively. The symbol ρ is the density of air (kg/m^3); C_P is the specific heat of air (J/(kg·K)); T_s and T_c are soil temperature (K) and vegetation canopy temperature (K), respectively; T_{ac} is the temperature in the canopy-air space (K); and T_a is air temperature (K) in the surface layer. The term r_x is the boundary layer resistance associated with the complete canopy of leaves (s/m), which is calculated according to Norman et al. (1995). The bulk aerodynamic resistance r_a (s/m) is calculated based on Monin-Obukhov surface layer similarity theory. The resistance to heat flow in the boundary layer immediately above the soil surface, r_s (s/m), is derived by Kustas and Norman (1999) as follows:

$$r_s = \frac{1}{c(T_s - T_c)^{1/3} + bu_s}, \tag{8}$$

where u_s is wind speed near soil surface (m/s). $c(T_s - T_c)^{1/3}$ is the free convection velocity (m/s). Kondo and Ishida (1997) indicated that c (m s^{-1} K$^{-1/3}$) ranges from 0.0011 for a smooth surface to 0.0038 for rough surface based on both laboratory and field experiments. The coefficient b (−) cannot be determined directly from routine observations, which relates to turbulent length scale in the canopy, soil surface roughness, and turbulence intensity (Sauer et al., 1995). The regression statistics for the rate of heat exchange over a soil surface beneath a maize canopy versus u_s from Sauer et al. (1995)'s experiments reported that b ranges from 0.025 to 0.087 during a whole growing season. For moderately rough soil surfaces, default values for b and c are 0.012 and 0.0025, respectively, in TSEB (Kustas & Norman, 1999). For rough soil surfaces with sparse vegetation, however, b and c are up to 0.087 and 0.0038 (Kondo & Ishida, 1997; Sauer et al., 1995), respectively. In a previous study (Kustas et al., 2016), $b = 0.065$ and $c = 0.0038$ were used for a strongly clumped tussock grassland with rocky soils in a semiarid region, yielding good agreement with measured H. This result is due to the fact that in sparsely vegetated semiarid and arid landscapes, accurate estimate of H_s is critical since it is the main contributor to H (Jacobs et al., 1996).

Radiometric surface temperature observations (T_R), the key variable for estimating surface energy fluxes based on TSEB, is partitioned into soil and vegetation component temperatures based on fraction vegetation cover (Kustas & Anderson, 2009):

$$T_R = \left[f_c(\theta)T_c^4 + (1 - f_c(\theta))T_s^4\right]^{1/4}, \tag{9}$$

where $f_c(\theta)$ is the vegetation cover fraction at the view angle θ of thermal sensor, and the soil and canopy temperatures, T_s and T_c, respectively, are estimated iteratively by solving equations (2)–(9) with an initial LE_c calculated based on PT formulation:

$$LE_c = \alpha_{PT} f_g \frac{\Delta}{\Delta + \gamma} R_{nc}, \tag{10}$$

where α_{PT} is PT coefficient of 1.26 assumed for unstressed transpiring vegetation. The value of α_{PT} is iteratively reduced for stressed vegetation conditions to achieve a physically plausible solution ($LE_s > 0$; see Kustas & Anderson, 2009). In equation (10), the variable f_g is the fraction of leaf area index (LAI) that is green, Δ is the slope of the saturation vapor pressure versus temperature curve (kPa/°C), and γ is the psychrometric constant (kPa/°C).

Surface energy fluxes and temperatures of the soil and vegetation are solved for iteratively with the above formulations. Model inputs for TSEB can be divided into two categories: meteorological forcing factors (i.e., air temperature, wind speed, vapor pressure, and incoming solar radiation) and land surface boundary conditions, the key ones being T_R, f_c, LAI, and canopy height (h_c). For more detailed description of TSEB, please refer to Norman et al. (1995) and Kustas and Norman (1999).

2.2. New Soil Resistance Formulation

Interactions between bluff-body elements, protruding a drying surface, and airflow boundary layer result in complex and unsteady flow regimes in the near-surface region forming a thin aerodynamic layer adjacent to the surface (termed viscous sublayer) that underlies turbulent air boundary layer and sets the upper boundary conditions for heat and water vapor transfer by thermal conduction and molecular diffusion, respectively (Haghighi et al., 2013; Haghighi & Or, 2013, 2015a, 2015c). The complex and unsteady flow regime is characterized by turbulent structures termed eddies (Palau-Salvador et al., 2010) that affect the viscous sublayer local patterns via modifying the local wind stress and drag partitioning and thus govern momentum, heat, and mass transfer processes (Haghighi & Kirchner, 2017; Haghighi & Or, 2015b; Raupach, 1992; Shao & Yang, 2008). Considering the dynamics of viscous sublayer caused by interactions between bluff-body elements and airflow, a mechanistic model for estimating turbulent sensible and latent heat fluxes over a drying surface with bluff-body elements, representing a natural landscape comprised of bare soil with rocks/stones and clumped vegetation, was proposed and verified using evaporation experiments conducted under controlled boundary conditions in a small wind tunnel (Haghighi & Or, 2015b). In this model, a boundary layer resistance r_{BL} (for the soil) was developed for heat transfer (s/m; Haghighi & Or, 2015c, 2015d), explicitly incorporating near-surface turbulence around dryland vegetation (Mayaud et al., 2016),

$$r_{BL} = \frac{\delta}{D_h}, \tag{11}$$

where D_h is thermal diffusivity of air ($\approx 1.9 \times 10^{-5}$ m^2/s; Decker et al., 2017) and δ (m) is the mean thickness of the viscous sublayer. Following Haghighi and Or (2013), δ is expressed as

$$\delta = g(\alpha)\frac{v}{u_*} \tag{12}$$

with a dimensionless coefficient $g(\alpha)$,

$$g(\alpha) = \frac{2.2\sqrt{112\pi}}{\Gamma(\alpha+1)}\frac{1}{2^{(\alpha+1)}\sqrt{\alpha+1}}\begin{cases} 1 & \alpha = 0 \\ \Pi(2\alpha+1) & \alpha > 0 \end{cases}, \tag{13a}$$

$$\Pi(2\alpha+1) = (2\alpha+1)(2(\alpha-1)+1)(2(\alpha-2)+1)\ldots(2(\alpha-n)+1) \quad n < \alpha, \tag{13b}$$

where v is the air kinematic viscosity (1.5×10^{-5} m^2/s) and n is the largest integer smaller than α. The variable α is the shape parameter of eddy residence time distribution, which can be determined from observations of spatially variable surface thermal fluctuations. With values of α typically ranging from 0 to 5, $g(\alpha)$ varies from 20.6 to 22.8 (Haghighi & Or, 2013). The friction velocity, u_* (m/s), is computed by (Haghighi & Or, 2013) as follows:

$$u_* = \frac{0.3}{\alpha+1}U_a, \tag{14}$$

where U_a is the mean wind speed at a reference height in the surface layer (m/s).

Shao and Yang (2008) developed a formulation for friction velocity (u_*) over rough surfaces (considered as a relatively smoother surface superposed with bluff-body elements), which is parameterized as

$$u_* = U_a\sqrt{f_r\lambda(1-\eta)C_{rg} + (f_s(1-\eta) + f_v\eta)C_{sg}}, \tag{15}$$

where η is the fraction of elements cover (equivalent to vegetation cover fraction, f_c) and λ is roughness density (or frontal area index) that can be calculated based on η, height of elements (h), and element width to height ratio (w_c/h_c; Haghighi & Or, 2015b; Shao & Yang, 2008). The variables f_r, f_s, and f_v are functions of quantities related to bluff-body elements parameterized by

$$f_r = \exp\left(-\frac{a_r\lambda}{(1-\eta)^k}\right), \tag{16}$$

$$f_s = \exp\left(-\frac{a_s\lambda}{(1-\eta)^k}\right), \tag{17}$$

$$f_v = 1 + \left(\frac{C_{sgc}}{C_{sg}} - 1\right)\eta, \tag{18}$$

where $a_r = 3$, $a_s = 5$, and $k = 0.1$ are determined from numerical simulations (Shao & Yang, 2008). The variables C_{rg}, C_{sg}, and C_{sgc} are drag coefficients for bluff-body element, ground surface, and surface of bluff-body element at $\lambda = 0$, respectively, which are defined as,

$$C_{sg} = \kappa^2 \ \ln^{-2}\left(\frac{z_w}{z_{0s}}\right), \tag{19}$$

$$C_{sgc} = \kappa^2 \ \ln^{-2}\left(\frac{z_w - h}{z_{0sc}}\right), \tag{20}$$

$$C_{rg} = \beta C_{sg}, \tag{21}$$

with

$$\beta = \frac{C_d}{\kappa^2}\left(\left(\ln\left(\frac{h}{z_{0s}}\right) - 1\right)^2 + 1\right), \tag{22}$$

where $\kappa = 0.41$ is the von Karman constant, z_w is the reference height (m) at which U_a is measured, z_{0s} is the roughness length for bare surface (m), z_{0sc} ($\approx z_{0s}$) is the roughness length for fully covered surface (m), h is the height for bluff-body element (m), and C_d is the drag coefficient of bluff-body element. For a wide range of plant species, C_d varies from 0.2 to 0.45 (Choudhury & Monteith, 1988; Gillies et al., 2002).

To generalize this model, Haghighi and Or (2015b) established a formulation for the average eddy distribution shape parameter $\overline{\alpha}$ for rough surfaces by combining equations (14) and (15),

$$\overline{\alpha} = \frac{0.3}{\sqrt{f_r\lambda(1-\eta)C_{rg} + (f_s(1-\eta) + f_v\eta)C_{sg}}} - 1, \tag{23}$$

where $\overline{\alpha}$ defined in eqaution (23) is independent of the thermal observations and parameterized as a function of bluff-body roughness density and drag coefficients that relate to interactions between near-surface turbulent airflow boundary layer and bluff-body elements (Haghighi & Or, 2015b; Mayaud et al., 2016).

Combining equations (11)–(13) with equations (15)–(23), the boundary layer resistance r_{BL} for heat transfer can be calculated over rough surfaces, which reflects physical insights about variations of eddy

Table 1
Input Parameters and Coefficients Involved in Calculating r_{BL}

Input parameter or coefficient		Description	Value source or value
Inputs	U_a	Mean air wind speed at reference height	Measurement
	z_w	Reference height for wind speed	Measurement
	η	Fraction of elements cover (i.e. f_c)	Measurement or calculate based on NDVI
	h	Height of elements (i.e. h_c)	Measurement or calculate based on NDVI
	w_c/h_c	Elements width to height ratio	1.5 in this study
Coefficients	z_{os}	Roughness length for bare surface	Ranges from 0.01 to 0.1 m for different sites
	C_d	Drag coefficient of bluff-body element	0.2 (Choudhury & Monteith, 1988)
	a_r	Model parameters	3 (Shao & Yang, 2008)
	a_s	Model parameters	5 (Shao & Yang, 2008)
	k	Model parameters	0.1 (Shao & Yang, 2008)

Note. NDVI = normalized difference vegetation index.

distribution (parameterized by eddy distribution shape parameter $\overline{\alpha}$) and patterns of momentum transfer to the surface (parameterized by friction velocity u_*). In this study, r_{BL} replaced r_s in equation (6) for estimating soil sensible heat flux H_s in TSEB for evaluating its performance in estimating the total sensible heat flux over semiarid and arid regions with sparse and clumped vegetation. Input parameters and coefficients involved in calculating r_{BL} are listed in Table 1.

3. Study Areas and Data Sets

Three semiarid and three arid sites were used in this study to evaluate the performance of TSEB with original and new soil resistance formulations. One semiarid site is in southeast Spain while the other two semiarid sites are in southwest United States. The three arid sites are in northwest China. A general description of the field sites is given in Table 2 (Garcia et al., 2013; Cheng et al., 2014; Li et al., 2008; Li et al., 2013; Scott, 2010, Scott et al., 2015; Xu et al., 2013). All six field sites are covered by sparse and clumped vegetation (Figure 1) and are under water-limited conditions. As a result, *ET* or *LE* rates are low, and *H* is the dominant turbulent flux during most of the growing season (Figure 2).

3.1. Semiarid Sites

The Balsa Blanca site is a tussock grassland located in Cabo de Gata National Park southwest of Spain with a semiarid Mediterranean climate characterized by rainy winters and dry summers. Although the study period is only part of a complete growing season, the data capture most of the annual variability in soil water availability, surface energy exchange, and phenology (Figure 2; Garcia et al., 2013; Morillas et al., 2013).

An EC system was installed at height of 3.5 m above ground level (agl) to measure sensible and latent heat fluxes with a sampling frequency of 10 Hz. The EC system was composed of a three-dimensional sonic anemometer (CSAT-3, Campbell Scientific Inc., Logan, UT, USA) that was used to measure wind speed and direction and an open-path infrared gas analyzer (LI-7500, LI-COR, Lincoln, NE, USA) that was used to measure water vapor and CO_2 concentration. (The use of trade, firm, or corporation names in this article is for the information and convenience of the reader. Such use does not constitute official endorsement or approval by the US Department of Agriculture or the Agricultural Research Service of any product or service to the exclusion of others that may be suitable.) The raw, high-frequency data were processed over 15-min intervals using the corrections for axis-rotation and density fluctuations (Garcia et al., 2013). Air temperature and relative humidity were measured by a thermo-hygrometer (HMP45C, Vaisala, Helsinki, Finland) installed at a height of 2.5 m agl. Net radiation and incoming shortwave radiation were measured using a net radiometer (NRLite, Kipp & Zonen, Delft, The Netherlands) installed at a height of 1.9 m and a LP02 Pyranometer (Campbell Scientific Inc., USA) at height of 3.5 m, agl respectively. A water-content reflectometer (ECHO EC5, Decagon Devices, Pullman, WA,USA) buried at depth of 0.04 m in a bare soil area was used to measure near-surface volumetric soil moisture content. Radiometric surface temperature, T_R, and soil surface temperature, T_s, were measured using Apogee broadband thermal infrared thermometers (IRTS-P, Apogee Instruments Inc., Logan, UT, USA). All the meteorological, soil water content, radiation, and temperature variables were averaged over 15-min intervals.

Table 2
A General Description of the Field Sites Used to Evaluate the TSEB Model With the Two Soil Resistance Formulations

	Semiarid sites			Arid sites		
	Balsa Blanca	Lucky Hills	Kendall	Desert steppe	Gobi	Sandy
Study period	15 Jan to 9 Jun in 2011	1 Jun to 30 Sep in 2013	1 Jun to 30 Sep in 2013	7 Jun to 14 Sep in 2012	1 Jun to 14Sep in 2012	2 Jun to 14 Sep in 2012
Latitude, longitude	36.94°N, 2.03°W	31.749°N, 110.052°W	31.737°N, 109.943°W	38.765°N, 100.318°E	38.915°N, 100.304°E	38.789°N, 100.493°E
Elevation (m)	196	1370	1530	1731	1562	1594
Annual precipitation (mm)	375	285	294	157	110	140
Mean air temperature (°C)	18.1	17.6	17.3	9.4	9.3	9.0
Land cover type	Grass	Shrub	Grass	Short shrub	Grass	Grass
Dominate species	*Stipa tenacissima*	*Parthenium incanum*, *Acacia constricta*, *Larrea tridentata*	*Eragrostis lehmanniana*, *Bouteloua eripoda*, *Aristida spp*	*Reaumuria soongaria*	*Alhagi sparsifolia*	*Artemisia ordosica*, *Scorzonera divaricata Turcz*, *Inula salsoloides*
h_c (m)[a]	0.7	1.0	0.3	0.3	0.2	0.3
Range of f_c[a]	0.6	0.05–0.22	0.07–0.31	0.11–0.32	0.10–0.18	0.09–0.22
Range of LAI[a]	1.05	0.10–0.50	0.15–0.75	0.15–0.78	0.20–0.38	0.19–0.50
Soil texture class (rock content)	Very gravelly sandy loams (high)	Gravelly sandy loams (high)	Very gravelly, sandy to fine sand, and clay loams (high)	Silt loams (moderate)	Silt loams (moderate)	Fine sand (none)
Values of z_{os} in TSEB	0.1	0.1	0.1	0.05	0.05	0.01

Note. LAI = leaf area index; TSEB = two-source energy balance.
[a]Values used for the study period.

Measured values of vegetation cover fraction (f_c) and canopy height (h_c) of 0.6 and 0.7 m, respectively, were considered as constant for the experimental period because the site was comprised of perennial grasses. Considering the fact that a significant amount of dead/senescent grass always exists in perennial tussock grass communities during the whole growing season, Kustas et al. (2016) assumed that total (green + dead) local LAI was a constant value of 1.75 based on visual observations. The fraction green vegetation, f_g, was derived based on green LAI calculated using an NDVI (normalized difference vegetation index)-LAI relationship derived from Tetracam camera images (ADC Tetracam Inc., Chatsworth, CA, USA) together with LAI from destructive sampling.

The other two semiarid sites, Lucky Hills and Kendall, are located in the U.S. Department of Agriculture-Agricultural Research Service Walnut Gulch Experimental Watershed, located southeast of Tucson, Arizona, USA (Scott, 2010; Scott et al., 2015). The climate is characterized by cool, dry winters and warm, wet summers, with 50–60% rainfall arriving in July–September as part of the North American Monsoon (Scott, 2010). Lucky Hills is a desert shrubland containing several species while Kendall is a semidesert grassland comprised mainly of grasses with a few scattered shrubs.

At each site, the EC flux tower, which is still in operation, contains EC, radiation, and meteorology instrumentation. The EC systems are mounted at ~5 m above the height of the vegetation with four-component radiation measurements at ~3 m above the canopy. Air temperature and relative humidity are made with temperature/relative humidity probe (HMP35C, Vaisala, Helsinki, Finland) at a height of 6 m agl. Wind speed and direction are measured at height of 6.4 m agl. Near surface volumetric soil water content at 0.05-m depth is measured by TDR soil moisture probes (CS616, Campbell Scientific Inc., Logan, UT, USA). These measurements were processed over 30-min intervals and are available at the AmeriFlux website (Lucky Hills site is named as US-whs, and the Kendall site is referred to as US-wkg).

Land surface temperature over the study sites was derived based on upwelling and downwelling longwave radiation measured by four-component radiometers using thermal radiative transfer theory (Liang, 2004). The constant values of h_c given by Li et al. (2008) were used in this study (i.e., 1 m for Lucky Hills and 0.3 m for Kendall). Values of f_c and LAI were calculated from NDVI using a relationship from Li et al. (2008). NDVI was calculated using fused red and near-infrared reflectance that was derived from 30-m Landsat 8 and 500-m Moderate Resolution Imaging Spectroradiometer images using the spatial and temporal adaptive reflectance fusion model (Gao et al., 2006).

3.2. Arid Sites

The Desert steppe, Gobi, and Sandy sites are located around an artificial oasis at the midpoint of the Heihe River Basin in northwest China. This region has an arid continental monsoon climate characterized by extremely hot summers and severely cold winters, with 60–70% of precipitation occurring in the summer months (Cheng et al., 2014). In 2012, a comprehensive eco-hydrological experiment—the Heihe Water Allied Telemetry Experimental Research project including the Multi-Scale Observation Experiment on Evapotranspiration (HiWATER-MUSOEXE)—was conducted in this region from May to September (Li et al., 2013; Xu et al., 2013). An

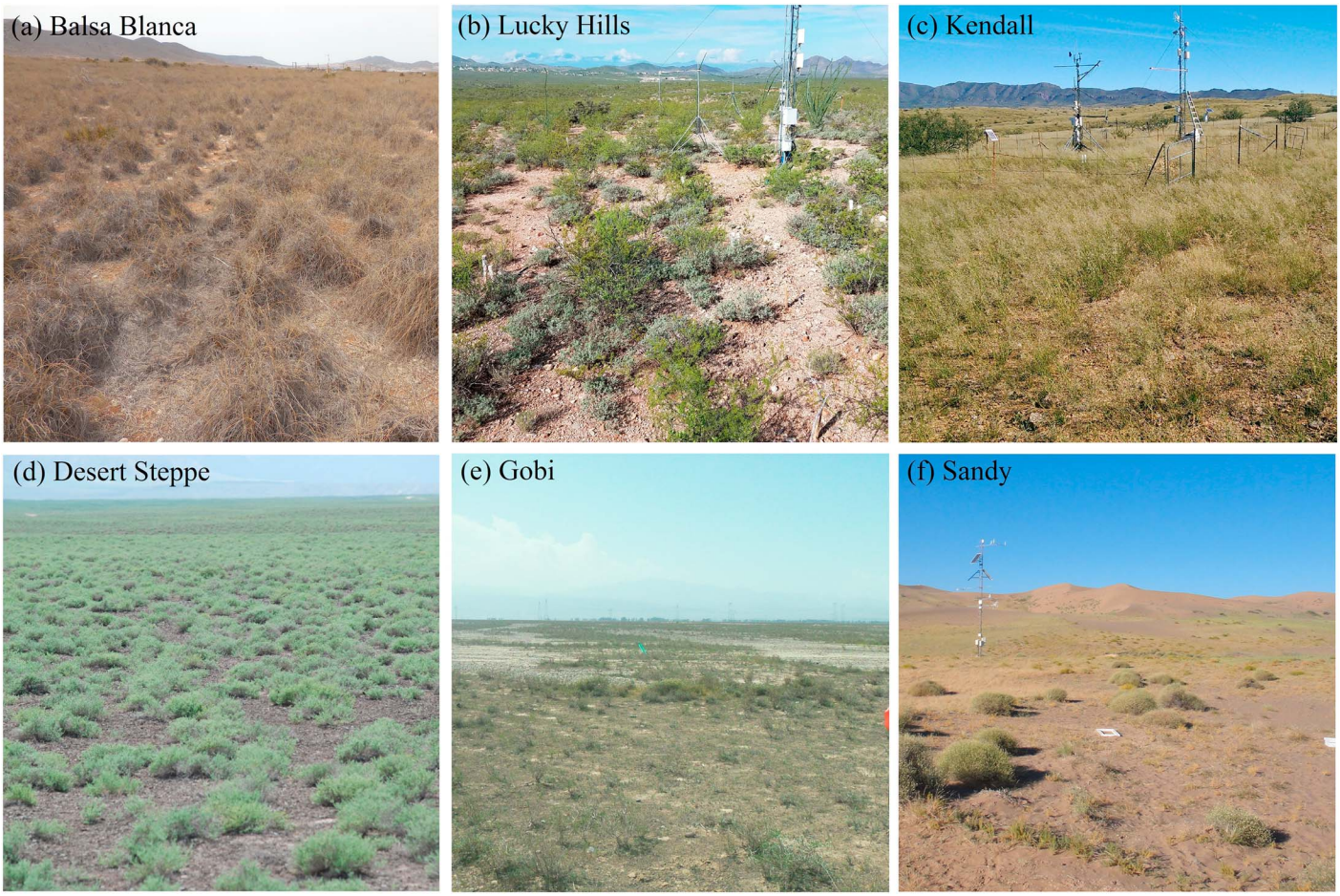

Figure 1. Photos of typical land cover conditions for the (a) Balsa Blanca, (b) Lucky Hills, (c) Kendall, (d) Desert steppe, (e) Gobi, and (f) Sandy sites.

extensive network of measurement sites including the three desert sites was instrumented during the HiWATER-MUSOEXE experiment. The meteorological and land surface flux observations collected from the HiWATER-MUSOEXE experiment are available at the Cold and Arid Regions Science Data Center at Lanzhou (http://card.westgis.ac.cn/).

For the Desert steppe site, the EC system is still in operation and is installed at height of 2.85 m agl. Humidity and temperature probes (HMP45A, Vaisala, Helsinki, Finland) are installed at three levels (1, 1.99, and 2.99 m agl). Wind speed and direction are made with wind sentry anemometer and vane (03102/03302, RM Young, Traverse City, MI, USA) systems at four levels (0.48, 0.98, 1.99, and 2.99 m agl). Air temperature, relative humidity, and wind speed measured at 2.99 m were used for this site. Four-component radiation measurements are made with a CNR1 radiometer (Kipp & Zonen, Delft, Netherlands) installed at height of 2.65 m agl. Volumetric soil moisture content is measured at a depth of 0.1 m using soil moisture sensor (ML2X, Delta-T Devices Ltd, Cambridge, UK) buried at 2 m south of the EC tower.

For the Gobi and Sandy desert sites, the EC systems (no longer operating after 2015) were installed at a height of 4.6 m agl. Air temperature, relative humidity, and wind speed were measured at two levels (5 and 10 m); the observations at 5 m agl were used in this study. A four-component radiometer (CNR1, Kipp & Zonen, Delft, Netherlands) was installed at 6 m agl. Soil moisture sensors (ECH_2O-5, Decagon Devices, Pullman, WA, USA, for the Gobi site, and CS616, Campbell Scientific Inc., Logan, UT, USA, for the Sandy site) were buried at seven levels (0.02, 0.04, 0.1, 0.2, 0.4, 0.6, and 1 m). Volumetric soil moisture measurements at 0.04 m were used in this study because the sampling at this depth was nearly time continuous. Composite land surface temperature was derived based on upwelling and downwelling longwave radiation measurements. Meteorological measurements and turbulent fluxes were processed over 30-min intervals.

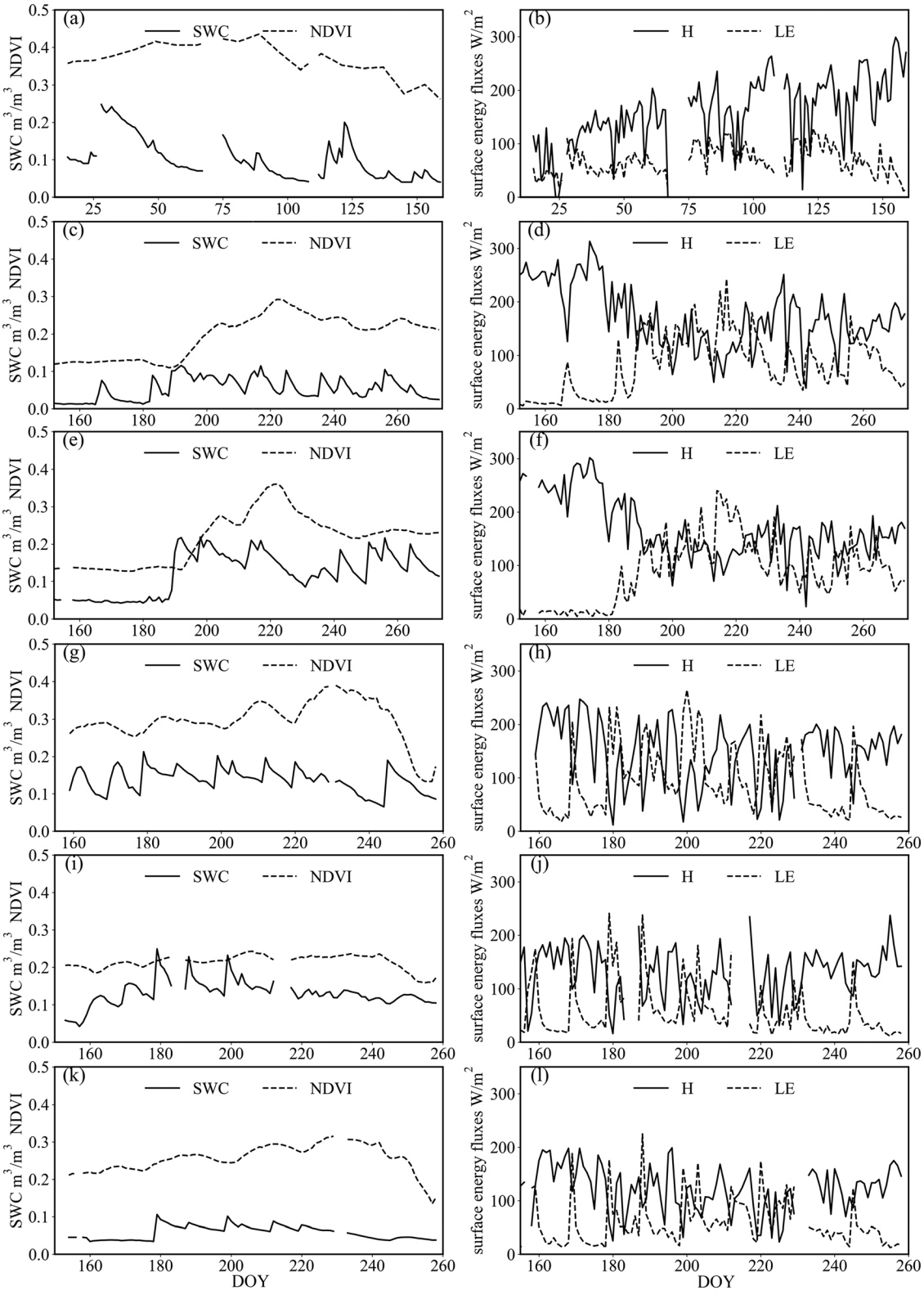

Figure 2. Variation in normalized difference vegetation index (NDVI), midday soil water content (SWC) at depths of 0.04 m for Balsa Blanca, Gobi, and Sandy; 0.05 m for Lucky Hills and Kendall; and 0.1 m for Desert steppe, and daytime average sensible and latent heat flux from the eddy covariance measurements during experiment periods used with TSEB model. Values for Balsa Blanca are shown in (a, b) and (c, d) for Lucky Hills, (e, f) for Kendall, (g, h) for Desert steppe site, (i, j) for Gobi, and (k, l) for Sandy site.

Desert steppe site is partially covered by small shrubs while Gobi and Sandy sites are partially covered by perennial grasses. Due to the fact that these three sites are dominated by perennial vegetation, h_c was considered as constant (h_c = 0.3 m for Desert steppe, 0.2 m for Gobi, and 0.3 m for Sandy) during the study period. Estimates of f_c were calculated via the NDVI-based approach proposed by Gutman and Ignatov (1998). LAI was derived from f_c using an exponential relationship between f_c and LAI (Choudhury, 1987). In this study, NDVI was calculated by fusing red and near-infrared reflectances at 90-m spatial resolution from Advanced Space-borne Thermal Emission Reflectance Radiometer with spatiotemporal characteristics at 500 m from Moderate Resolution Imaging Spectroradiometer (Li et al., 2017). Estimates of f_g were computed as the ratio of fraction of photosynthetically active radiation absorbed by green vegetation cover (f_{APAR}) and intercepted by total vegetation cover (f_{IPAR}; Fisher et al., 2008).

4. Evaluating TSEB Model Performance

4.1. Evaluation Strategy

Sensible (H) and latent (LE) heat fluxes obtained from an EC system, net radiation (R_n) measured with a radiometer, and soil heat flux (G) calculated from an array of soil heat flux plates and near-surface soil temperature and moisture measurements are widely used to validate the performance of ET models. However, the sum of H and LE from EC is generally less than available energy ($R_n - G$), known as surface energy imbalance or lack of energy closure. There are many factors that can contribute to this flux mismatch, including a mismatch in source areas between the EC turbulent measurements of H and LE, and the net radiometer, and soil heat flux measurements, ignoring or underestimating the heat storage terms, neglecting advective flux divergence, and inability to capture large eddies using EC systems (Foken, 2008; Leuning et al., 2012; Xu et al., 2017).

Average values of the closure ratios $(H + LE)/(R_n - G)$ during the study periods for Balsa Blanca, Lucky Hills, Kendall, Desert steppe, Gobi, and Sandy were 0.8 (Morillas et al., 2013), 0.8 and 0.75 (Scott, 2010), 0.88, 0.86, and 0.76 (Li et al., 2017), respectively. The impact of energy imbalance on model comparisons can be assessed by forcing closure in the observed energy budget. Given that underestimation of LE relative to H tends to be considered the main reason for energy imbalance (Wang & Dickinson, 2012), the residual-LE closure method is considered as the most appropriate method for validating SEB-based models in previous studies (Alfieri et al., 2012; Li et al., 2005; Li et al., 2017; Morillas et al., 2013; Song et al., 2016). This method assumes that H is measured accurately and adjusts LE by adding residual of energy balance (i.e., $R_n - G - H = LE$). However, there is mounting evidence of sonic anemometer measurement issues (Frank et al., 2013; Kochendorfer et al., 2012), which affect both H and LE. But in these sparsely vegetated environments, G is a significant term in the energy balance, similar in magnitude to H. Hence, the method for measuring G can significantly affect its magnitude (e.g., Liebethal et al., 2005; Ochsner et al., 2006). In addition, the sparse and heterogeneous nature of arid vegetated landscapes makes it challenging to obtain an areal average G representative of the tower flux footprint (Kustas et al., 2000). Considering the objective of this study, and the energy balance closure issues discussed above—namely, evaluating the performance of the TSEB using different soil resistance formulations—only the sensible heat flux, which has its main contribution from the soil (H_s), was evaluated here since it tends to be more accurately measured and is a direct computation in TSEB.

In addition to the traditional method of evaluating TSEB by comparing with observed H from EC systems, a new model evaluation strategy—benchmarking model performance—proposed by Best et al. (2015) was used to evaluate TSEB performance. Best et al. (2015) reported that unlike traditional methods of model evaluation, benchmarking model performance can lead to different conclusions about model performance based on setting expectations of performance (i.e. performance benchmarks) for a range of metrics. In benchmarking model performance strategy, simple physically based models as well as empirical relationships can be used as the benchmarks. The metrics (i.e., error statistics) for all models and benchmarks are determined by comparing observations and model output. Then, each model is ranked, with the best performant given a score of 1 and the worst a score of 5 in this study. Finally, the average rankings for each model over all statistics and all sites are given as

$$\overline{R_i} = \frac{1}{n_s n_t} \sum_{j=1}^{n_s} \sum_{k=1}^{n_t} R_{jik}, \tag{24}$$

where $\overline{R_i}$ is the average ranking for ith model or benchmark, n_s is the number of study sites, n_t is the number of statistical metric, and R_{jik} is the ranking of ith model or benchmark at site j for statistical metric k. The average rankings for models are reasonably robust because the influence of a particularly good or poor performance on overall average rankings is avoided with limited contribution from each statistic at each site (Best et al., 2015).

For this study, a simple one-source surface energy balance (OSEB) model (Kustas et al., 1996) was considered as the benchmark. Total H from the combined soil-canopy system can be governed by a bulk resistance formulation,

$$H = \rho C_P \frac{T_r - T_a}{r_{ah}}, \tag{25}$$

with

$$r_{ah} = \frac{1}{ku^2}\left[\ln\left(\frac{z-d_0}{z_{om}}\right) - \Psi_m\right]\left[\ln\left(\frac{z-d_0}{z_{om}}\right) + kB^{-1} - \Psi_h\right], \tag{26}$$

where T_r is composite radiometric surface temperature (K), r_{ah} is the resistance for heat transfer (s/m), u is wind speed (m/s) at reference height z (m), z_{om} is roughness heights for momentum transfer (m), and Ψ_m and Ψ_h are the stability corrections for momentum and heat transfer, respectively. The variable kB^{-1} (−) represents the difference in the efficiency of heat and momentum transport. For semiarid and arid regions, an average value of $kB^{-1} = 7$ was derived from equations (25) and (26) using observed H, u, T_r, and T_a by Stewart et al. (1994). For the six study sites in this case, however, the average value of $kB^{-1} = 3.7$ was derived from a similar set of observations.

Here the OSEB with $kB^{-1} = 7$ is set as a *better-than-another* benchmark (Best et al., 2015), which means that the more complicated physically based TSEB should outperform this benchmark validating the hypothesis that TSEB is a more robust model than OSEB in semiarid/arid environments. The OSEB with $kB^{-1} = 3.7$ is set as a *fit-for-a-particular-application* benchmark (Best et al., 2015) that represents the level of performance required for TSEB to meet or exceed to be considered an improvement over existing approaches.

4.2. Model Sensitivity Analysis

To identify the sensitivity of input variables and coefficients in the soil resistance formulations used in $TSEB_{KN}$ (i.e., TSEB with soil resistance formulation proposed by Kustas & Norman, 1999) and $TSEB_{HO}$ (i.e., TSEB with soil resistance formulation proposed by Haghighi & Or, 2015b, 2015d), the Extended Fourier Amplitude Sensitivity Test (EFAST) was used for global sensitivity analysis. The EFAST method developed by Saltelli et al. (1999) not only computes the main effect contribution of each individual factor to the variance of the output but also addresses the influence of the interactions between factors on the variance of the model predictions. For each factor i, there are two sensitivity indexes derived from EFAST: (1) the first order effect index (S_i) and (2) the total effect index (S_{Ti}). The S_i measures the influence of factor i without considering interactions with other factors, which is defined as

$$S_i = \frac{Var_{Xi}[M(Y/X_i)]}{Var(Y)}, \tag{27}$$

where Y denotes the output variable and X_i denotes the factor i. Var and M are the variance operator and the expectancy operator, respectively.

The variable S_{Ti} indicates the total effect of factor i on the output variance considering its main effect as well as interactions with other factors. The S_{Ti} is expressed as

$$S_{Ti} = S_i + S_{ij} + S_{ijm} + \cdots + S_{1,2,\cdots,i,\cdots,k}, \tag{28}$$

Table 3
The Sensitivity Indexes of Model Coefficients and Range in Input Variables or Coefficients for Estimating H Using $TSEB_{KN}$

Inputs or coefficients		The sensitivity indexes	
Names	Ranges	S_i	STi
f_c	[0.05, 0.6]	0.05	0.26
LAI	[0.10, 1.05]	0.10	0.34
h_c	[0.2, 1.0]	0.12	0.27
w_c/h_c	[0.5, 2.0]	0	0.03
z_{os}	[0.01, 0.1]	0	0.06
b	[0.012, 0.087]	0.34	0.58
c	[0.0011, 0.0038]	0.08	0.18

where S_{ij} is the second-order sensitivity index for factor i, measuring the contributions of the interaction between factors i and j to output variance. Similarity, S_{ijm} and $S_{1,2,\cdots,i,\cdots,k}$ are the third-order and higher-order sensitivity index. The difference between S_{Ti} and S_i represents the interactions among factors.

In this study, the sensitivity of H to input variables and coefficients used in the soil resistance formulations were calculated using EFAST from an open-source Python library for Sensitivity Analysis (SALib; Herman & Usher, 2017). The input parameters related to resistance terms for $TSEB_{KN}$ and $TSEB_{HO}$ usually derived from satellite data with relatively large uncertainty include LAI, f_c, and h_c and therefore were used in this sensitivity analysis. The input parameters w_c/h_c and z_{os} were also analyzed, which are usually considered as constant when running TSEB. Additionally, variation in the soil resistance coefficients b and c in equation (8) was analyzed for $TSEB_{KN}$. For $TSEB_{HO}$, variation in the soil resistance coefficients listed in Table 1 was evaluated in the sensitivity analysis. For each input or coefficient, 7,000 samples were generated and analyzed in EFAST. The sampling range of LAI, f_c, h_c, and z_{0s} were determined based on the observed range in their values for the six sites listed in Table 2. The range in values of the soil resistance coefficients for $TSEB_{KN}$ and $TSEB_{HO}$ was derived from the literature (Choudhury & Monteith, 1988; Gillies et al., 2002; Kondo & Ishida, 1997; Kustas & Norman, 1999; Sauer et al., 1995; Shao & Yang, 2008). The sampling range for all analyzed inputs and coefficients are listed in Tables 3 and 4.

5. Results

5.1. Sensitivity Analysis

The sensitivity indexes of H from $TSEB_{KN}$ and $TSEB_{HO}$ are presented in Figure 3 and Tables 3 and 4. From Figure 3a and Table 3, it appears that $TSEB_{KN}$ has relatively low sensitivity to w_c/h_c and z_{os} with S_i of~0 and S_{Ti} less than 0.06. However, the sensitivity analysis indicates that coefficient b is a highly sensitive parameter for computing H yielding S_i of 0.34 and S_{Ti} of 0.58. In addition, $TSEB_{KN}$ shows moderate sensitivity to vegetation parameters LAI, f_c, h_c, and coefficient c with S_i between 0.05 and 0.12 and S_{Ti} between 0.18 and 0.34. For almost all analyzed parameters and coefficients used in $TSEB_{KN}$, the second- and higher-order interactions among the 7 factors (i.e., $S_{Ti} - S_i$) had a larger impact on H than the effects of any individual factor. With the new soil resistance formulation in TSEB, namely, $TSEB_{HO}$, variation in f_c and h_c had a moderate effect on H estimates with S_i of~0.15 and S_{Ti} of~0.25, while variation in w_c/h_c and z_{os} did not significantly affect H estimates with S_{Ti} less than 0.02 (Figure 3b and Table 4). This is similar to the results found with $TSEB_{KN}$. It appears that the value of a_r may cause the largest variations in $TSEB_{HO}$ estimates of H but in all cases S_{Ti} values are below 0.1, indicating $TSEB_{HO}$ has relatively low sensitivity to all the soil resistance model coefficients. $TSEB_{HO}$ shows highest sensitivity to LAI yielding S_i of 0.45 and S_{Ti} of 0.52, similar to the sensitivity of the soil resistance coefficient b for $TSEB_{KN}$. However, interactions among factors had relatively lower impact on estimates of H using $TSEB_{HO}$ versus $TSEB_{KN}$. Therefore, compared with $TSEB_{KN}$, $TSEB_{HO}$ appears to be more robust because interactions among input variables and uncertainty in key coefficients do not lead to significant variation in modeled estimates of H.

Table 4
The Sensitivity Indexes of Model Coefficients Range in and Input Variables or Coefficients for Estimating H Using $TSEB_{HO}$

Inputs or coefficients		The sensitivity indexes	
Names	Ranges	S_i	S_{Ti}
f_c	[0.05, 0.6]	0.15	0.25
LAI	[0.10, 1.05]	0.45	0.52
h_c	[0.2, 1.0]	0.17	0.22
w_c/h_c	[0.5, 2.0]	0	0.01
z_{os}	[0.01, 0.1]	0	0.02
C_d	[0.2, 0.45]	0	0.01
a_r	[0.0, 10.0]	0.06	0.09
a_s	[0.0, 10.0]	0.02	0.03
k	[0.0, 1.0]	0	0.01

5.2. Performance of TSEB With Different Soil Resistance Formulations

The TSEB model has not been extensively applied and verified over heterogeneous semiarid and arid regions, which are challenging landscapes for estimating surface fluxes due to random and ill-defined canopy cover, large differences in the efficiency in heat flux transport from the soil and vegetation canopy surfaces, and major contribution of the

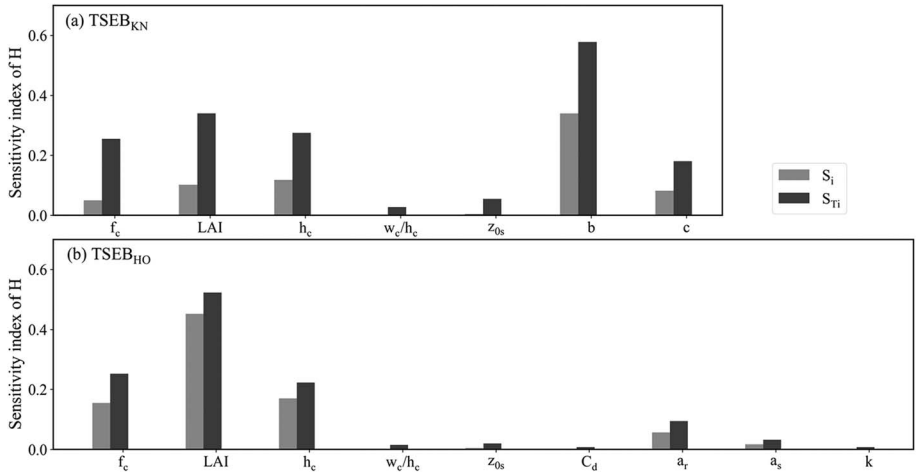

Figure 3. The sensitivity indexes for *H* from TSEB$_{KN}$ (a) and TSEB$_{HO}$ (b) due to uncertainty in model parameters and key input variables. TSEB = two-source energy balance.

soil component to the turbulent fluxes, particularly *H*. To evaluate performance of TSEB with different soil resistance formulations over these heterogeneous semiarid and arid sites as discussed in section 4.1, modeled *H* from TSEB was compared with measured *H* from the EC systems at all six study sites, as shown in Figure 4. Quantitative measures (i.e., error statistics) of modeled *H* for the six study sites are listed in Table 5.

As reported by Kustas et al. (2016), TSEB$_{KN}$ with original soil resistance coefficients b = 0.012 and c = 0.0025 clearly underestimated *H* with a significant bias (Figure 4a) for Balsa Blanca, which contained rocky and rough soil surface with clumped vegetation, while reliable estimates of *H* were recomputed using b = 0.065 and c = 0.0038 with points scattered around the 1:1 line (Figure 4b). For the other five study sites, *H* was also underestimated by TSEB$_{KN}$ with original soil resistance coefficients, yielding large bias values for Lucky Hills, Kendall, and Desert Steppe (Figures 4d, 4g, and 4j). According to ground observations (Table 2 and Figures 1 and 2), the Lucky Hills, Kendall, and Desert Steppe are similar in soil roughness and vegetation distribution to Balsa Blanca while the Gobi, and Sandy sites have a much smoother soil surface and very sparse and short vegetation cover. Therefore, improvement in the agreement with *H* observations using TSEB$_{KN}$ was expected using b = 0.065 and c = 0.0038 for Lucky Hills, Kendall, and Desert Steppe. Thus, TSEB$_{KN}$ computed *H* with b = 0.065 and c = 0.0038 was compared with observations, and results are shown in Figures 4b, 4e, 4h, 4k, 4n, and 4q. Indeed, the agreement with observed *H* improved for Lucky Hills, Kendall, and Desert Steppe using the larger coefficients. The values of bias, root mean square error, and the mean absolute percent difference (MAPD) are reduced. However, the most significant improvement in model performance by adjusting b and c is still with the Balsa Blanca site. For Sandy and Gobi sites, TSEB$_{KN}$ with the default b and c produces quite reliable estimates of *H* with higher coefficient of determination (R^2) and Nash-Sutcliffe efficiency coefficient values. The good results using the default values for b and c for Gobi and Sandy sites is likely because these sites have smoother soil surfaces with lower fractional cover and smaller vegetation.

The results from the sensitivity analysis and estimates of *H* using TSEB$_{KN}$ suggest that reasonable estimates of *H* can be computed if soil resistance coefficients b and c can be modified based on ground/land use information when applied over these sparsely vegetated heterogeneous landscapes. Since b and c cannot be determined directly from routine satellite observations, adjusting b and c coefficients for specific study areas would be a major challenge, operationally, especially over complex landscapes. Yet basic land cover information may help to nominally adjust b and c values in different arid regions.

A similar comparison of modeled versus measured *H* using TSEB$_{HO}$ over these same semiarid and arid sites is shown in Figure 4. The coefficients of r_{BL} is listed in Tables 1 and 2, which did not significantly affect *H* estimates. It is clear from Figure 4 and the statistics in Table 5 that TSEB$_{HO}$ performs quite

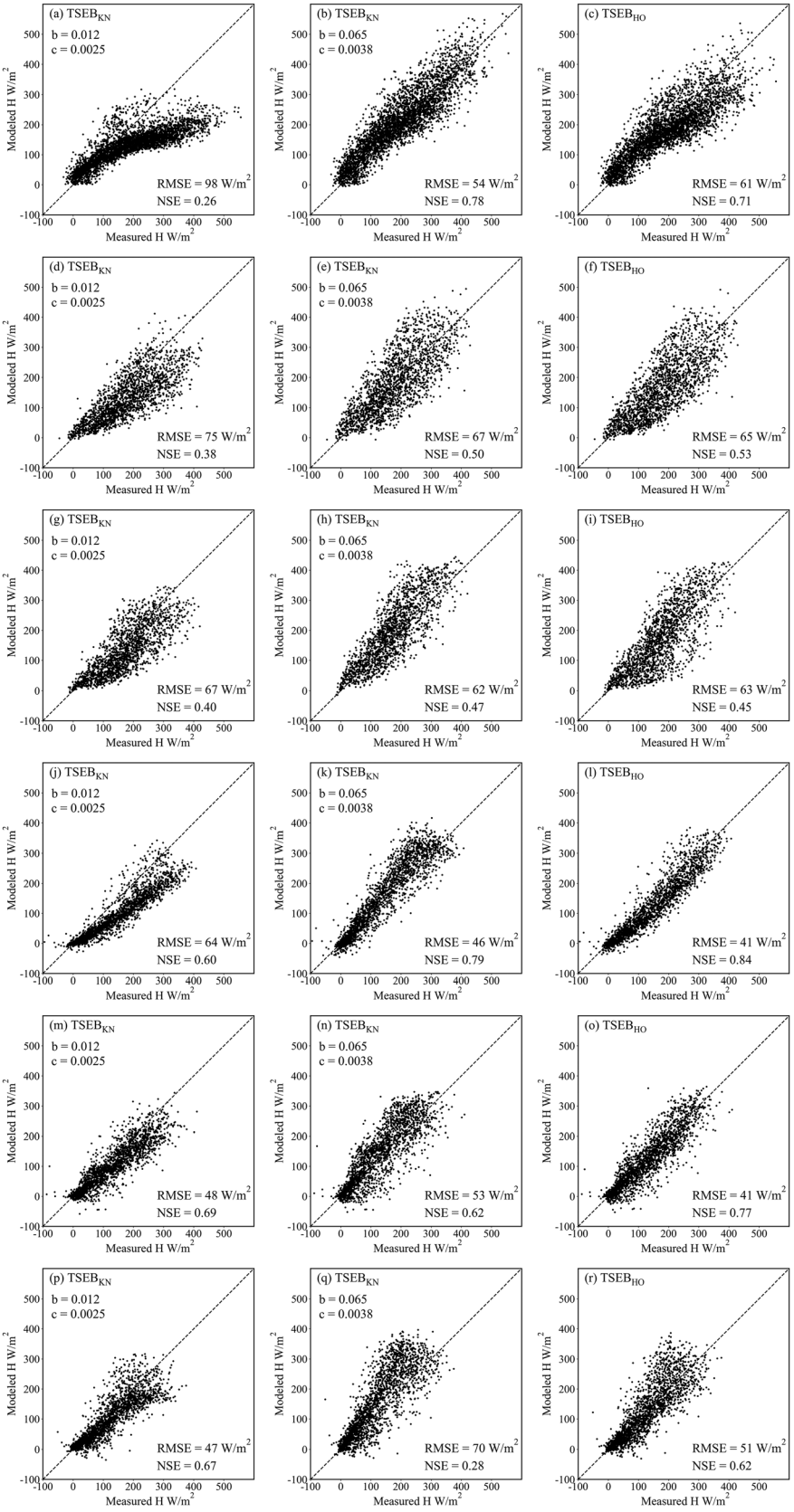

Figure 4. Comparisons of measured *H* from EC systems and modeled *H* from $TSEB_{KN}$ with original and modified coefficients and from $TSEB_{HO}$ for (a–c) Balsa Blanca, Lucky (d–f) Hills, (g–i) Kendall, (j–l) Desert steppe, (m–o) Gobi, and (p–r) Sandy sites.

Table 5
Statistical Results Comparing Modeled H From $TSEB_{KN}$ With Original and Modified Coefficients and $TSEB_{HO}$ With Measurements for Balsa Blanca, Lucky Hills, Kendall, Desert steppe, Gobi, and Sandy Experimental Sites

	$TSEB_{KN}$ with b = 0.012 and c = 0.0025					$TSEB_{KN}$ with b = 0.065 and c = 0.0038					$TSEB_{HO}$				
Study sites	Bias	RMSE	MAPD	R^2	NSE	Bias	RMSE	MAPD	R^2	NSE	Bias	RMSE	MAPD	R^2	NSE
Balsa Blanca	−61	98	39	0.65	0.26	14	54	22	0.81	0.78	−23	61	24	0.76	0.71
Lucky Hills	−46	75	33	0.61	0.38	4	67	29	0.6	0.5	−13	65	29	0.62	0.53
Kendall	−39	67	31	0.62	0.4	23	62	28	0.69	0.47	−4	63	28	0.63	0.45
Desert Steppe	−48	64	36	0.85	0.6	15	46	23	0.86	0.79	−22	41	22	0.89	0.84
Gobi	−27	48	28	0.79	0.69	12	53	31	0.72	0.62	−7	41	23	0.80	0.77
Sandy	−19	47	28	0.73	0.67	33	70	43	0.69	0.28	0	51	30	0.71	0.62

Note. Bias is the average difference between measured and modeled H (W/m^2); RMSE is root mean square error (W/m^2); MAPD (%) is mean absolute percent difference (average of absolute difference between modeled and measured H divided by average measured H); R^2 is the coefficient determination. NSE is the Nash-Sutcliffe efficiency coefficient.

well for all the sites with points distributed around the 1:1 line and the Nash-Sutcliffe efficiency value ranging from 0.45 to 0.84. For Balsa Blanca, $TSEB_{HO}$ yields a bias and root mean square error values slightly larger than that of $TSEB_{KN}$ with modified soil resistance coefficients (Table 5) but clearly less than that of $TSEB_{KN}$ with original coefficients (Kustas et al., 2016; Morillas et al., 2013). For Lucky Hills and Kendall, $TSEB_{HO}$ performance is similar to $TSEB_{KN}$ with modified soil resistance coefficients but, again, is better than $TSEB_{KN}$ using original soil resistance coefficients. For Desert steppe and Gobi sites, $TSEB_{HO}$ performance is slightly better than $TSEB_{KN}$. For the Sandy site, the errors in H for $TSEB_{HO}$ are similar to $TSEB_{KN}$ with original soil resistance coefficients but with H slightly underestimated by $TSEB_{KN}$ and slightly overestimated by $TSEB_{HO}$ when H is greater than 200 W/m^2. MAPD values from $TSEB_{HO}$ and $TSEB_{KN}$ with coefficients b and c adjusted for the soil/vegetation condition range between 20% and 30%. This range in MAPD values is similar to the uncertainty in the EC observations evaluated for these study sites, which is 10% to 30% for Lucky Hills and Kendall (Scott, 2010), and nearly 20% reported for the three arid sites (i.e., Desert Steppe, Gobi, and Sandy; Wang et al., 2015) and for Balsa Blanca (Morillas et al., 2013).

To test the hypothesis of TSEB being a superior model and to evaluate the improvements made by modifying soil resistance formulations in general, the average rankings of TSEB with different soil resistance formulations and two benchmarks were calculated across the six study sites, with the results summarized in Table 6. Overall, TSEB with original soil resistance coefficients b = 0.012 and c = 0.0025 outperforms OSEB with kB^{-1} = 7 (the better-than-another benchmark), which is the minimum expectation TSEB should meet. However, the $\overline{R}$ of TSEB with original coefficients is much greater than OSEB with kB^{-1} = 3.7 (the *fit-for-a-particular-application* benchmark), indicating the need for improving the performance of original TSEB in semiarid and arid regions. The $\overline{R}$ of $TSEB_{KN}$ with b and c adjusted for site soil/vegetation roughness and $TSEB_{HO}$ are 1.81 and 1.89, respectively, which are much smaller than $\overline{R}$ of the better-than-another benchmark (3.69) and of original TSEB (2.92) and slightly less than the $\overline{R}$ value of the fit-for-a-particular-application benchmark (1.91). This implies that both modifications to the soil resistance term (i.e., either adjusting coefficients in the original soil resistance formulation or introducing the new physically based soil resistance formulation in TSEB) are viable options for improving the performance of TSEB in semiarid and arid regions.

Table 6
Average Rankings of Benchmarks and TSEB Models for the Statistics (Bias, RMSE, MAPD, R^2, and NSE) Across All Six Study Sites

	$TSEB_{KN}$ with b = 0.012 c = 0.0025	$TSEB_{KN}$ with adjusted b and c[a]	$TSEB_{HO}$	OSEB with kB^{-1} = 7	OSEB with kB^{-1} = 3.7
Average ranking	2.92	1.81	1.89	3.69	1.91

MAPD = mean absolute percent difference; NSE = Nash-Sutcliffe efficiency;
[a] b = 0.065 and c = 0.0038 for balsa Blanca, Lucky Hills, Kendall, and desert steppe, and b = 0.012 and c = 0.0025 for Gobi and Sandy

6. Summary and Conclusions

This study evaluates the performance of thermal-based TSEB model applied to sparsely vegetated sites using EC measurements. Notwithstanding the many applications of TSEB model and its success in field tests, estimates of ET remain prone to bias in sparsely vegetated ecosystems where soil surface interactions are known to play a critical role. We implement insights from a newly proposed soil resistance formulation (Haghighi & Or, 2015b; $TSEB_{HO}$) that explicitly incorporates near-surface physical interactions governing surface heat fluxes and evaluate the performance of TSEB using original soil resistance formulation (Kustas & Norman, 1999) with coefficients modified for soil and canopy roughness ($TSEB_{KN}$) and the new physically based soil resistance scheme ($TSEB_{HO}$) that requires minimal adjustments for soil and canopy properties.

To evaluate the uncertainty in modeled sensible heat fluxes (H) from $TSEB_{KN}$ and $TSEB_{HO}$ incorporating the original and the newly proposed soil resistance formulations, respectively, a global sensitivity analysis was conducted for the key inputs and coefficients related to the resistance terms. The analysis indicated that $TSEB_{KN}$ has moderate sensitivity to vegetation parameters as well as $TSEB_{HO}$. However, $TSEB_{KN}$ output is highly sensitive to the soil resistance coefficients while $TSEB_{HO}$ has relatively low sensitivity to virtually all of its soil resistance coefficients. In addition, interactions among the inputs and coefficients of $TSEB_{KN}$ had higher contributions to the variance in H than that of $TSEB_{HO}$. This result indicates that improving estimates of H in $TSEB_{KN}$ will require appropriate soil resistance coefficients b and c estimated based on land cover information over sparely vegetated semiarid and arid regions. On the other hand, the new soil resistance formulation used in TSEB, $TSEB_{HO}$, appears to require little if any modification to its model coefficients and thus is less sensitive to interactions among input variables and associated uncertainties in the key coefficients.

We further tested the performance of $TSEB_{KN}$ with modified soil resistance coefficients based on soil and vegetation roughness characteristics and $TSEB_{HO}$ for estimating H using EC measurements from six arid and semiarid study sites. By adjusting the b and c coefficients for the clumped canopy layer with rough (rocky) soil surface as described in Kustas et al. (2016), $TSEB_{KN}$ performed well over Balsa Blanca (Spain), Lucky Hills (Arizona, USA), Kendall (Arizona, USA), and Desert steppe (China), with differences in model versus observed H similar to the measurement uncertainty. For smooth soil surfaces with very sparse and open canopies at the Gobi and Sandy sites (China), $TSEB_{KN}$ produced reasonable estimates of H with default values of soil resistance coefficients. The estimates of H from $TSEB_{HO}$ without making any changes to the default values for the soil resistance coefficients agreed well with the observations over all the six study sites with MAPD values ranging from 20% to 30% similar to or only slightly greater than the measurement uncertainty. The results of ranking $TSEB_{KN}$ with different soil resistance coefficients, $TSEB_{HO}$, and two benchmarks based on the OSEB model further confirm that $TSEB_{KN}$ with modified soil resistance coefficients and $TSEB_{HO}$ outperform OSEB models and $TSEB_{KN}$ using only the default values for the soil resistance coefficients for all semiarid and arid study sites.

The default values for the coefficients b and c in the soil resistance algorithm in $TSEB_{KN}$ are currently applied over most landscapes in the satellite-based regional model—Atmosphere Land-Exchange Inverse (ALEXI) and associated disaggregation scheme (DisALEXI; Anderson et al., 1997; Anderson et al., 2011). The results here indicate that when using the $TSEB_{KN}$ land surface scheme, that ALEXI/DisALEXI will likely need to modify the soil resistance coefficients in arid and semiarid landscapes with rough soil surfaces combined with strongly clumped vegetation (Kustas et al., 2016). Alternatively, adopting the $TSEB_{HO}$ land surface scheme within the ALEXI/DisALEXI modeling framework can potentially enhance its operational capabilities, requiring minimal ground information and providing more reliable estimates in these sparsely vegetated regions.

Future plans include evaluating the utility of $TSEB_{KN}$ and $TSEB_{HO}$ for estimating ET and soil evaporation (E) and canopy transpiration (T) over a wider range of climates and land cover types. This will require soil E observations using microlysimeters, and T estimates from sap-flow, and E/ET partitioning from isotopic analyses. The flux partitioning method using high-frequency EC data will also be employed (e.g., Scanlon & Kustas, 2012). Additionally, in future studies estimates of ET and surface energy fluxes using land surface temperature derived from satellite platforms in ALEXI/DisALEXI over semiarid and arid landscapes based on $TSEB_{HO}$ will be implemented and compared with the $TSEB_{KN}$ soil resistance formulation along with flux tower measurements for validation. This will provide a physical framework for improving estimates of ET partitioning into E and T components, which currently remote sensing-based models compute with significant uncertainty (Talsma et al., 2018).

Acknowledgments

The authors thank all the scientist, engineers, and students who conducted experiments in experimental sites. Data for Desert steppe, Gobi, and Sandy sites are available at the Cold and Arid Regions Science Data Center at Lanzhou (http://card.westgis.ac.cn/). Data for Lucky Hills and Kendall are available from AmeriFlux (Lucky Hills: https://doi.org/10.17190/AMF/1246113 and Kendall: https://doi.org/10.17190/AMF/1246112). C. H. acknowledges funding by the Strategic Priority Research Program of Chinese Academy of Sciences (Grant XDA19040504). E. H. is funded by the Swiss National Science Foundation fellowship (SNSF Grant P2EZP2-165244). M. G acknowledges funding from the EU and Innovation Fund Denmark in the frame of the collaborative international consortium FORWARD financed under the ERA-NET Cofund WaterWorks2015 Call (Water JPI). This ERA-NET is an integral part of the 2016 Joint Activities developed by the Water Challenges for a Changing World Joint Programme Initiative (Water JPI). F. D. acknowledges funding by the DINCOS project (CGL2016-78075-P) funded by the Spanish Ministry of Science and Innovation. Data for Balsa Blanca site is available by contacting the PI of the field site (F. D. at poveda@eeza.csic.es). USDA is an equal opportunity employer and provider.

References

Alfieri, J. G., Kustas, W. P., Prueger, J. H., Hipps, L. E., Evett, S. R., et al. (2012). On the discrepancy between eddy covariance and lysimetry-based surface flux measurements under strongly advective conditions. *Advances in Water Resources*, *50*, 62–78. https://doi.org/10.1016/j.advwatres.2012.07.008

Anderson, M. C., Kustas, W. P., Norman, J. M., & Hain, C. R. (2011). Mapping daily evapotranspiration at field to global scales using geostationary and polar orbiting satellite imagery. *Hydrology and Earth System Sciences*, *15*(1), 223–239. https://doi.org/10.5194/hess-15-223-2011

Anderson, M. C., Norman, J. M., Diak, G. R., Kustas, W. P., & Mecikalski, J. R. (1997). A two-source time-integrated model for estimating surface fluxes using thermal infrared remote sensing. *Remote Sensing of Environment*, *60*(2), 195–216. https://doi.org/10.1016/S0034-4257(96)00215-5

Best, M. J., Abramowitz, G., Johnson, H. R., Pitman, A. J., Balsamo, G., et al. (2015). The plumbing of land surface models: Benchmarking model performance. *Journal of Hydrometeorology*, *16*(3), 1425–1442. https://doi.org/10.1175/JHM-D-14-0158.1

Campbell, G. S., & Norman, J. M. (1998). *An introduction to environmental biophysics* (p. 286). New York: Springer. https://doi.org/10.1007/978-1-4612-1626-1

Cheng, G., Li, X., Zhao, W., Xu, Z., Feng, Q., Xiao, S., & Xiao, H. (2014). Integrated study of the water-ecosystem-economy in the Heihe River Basin. *National Science Review*, *1*(3), 413–428. https://doi.org/10.1093/nsr/nwu017

Choudhury, B. J. (1987). Relationships between vegetation indices, radiation absorption, and net photosynthesis evaluated by a sensitivity analysis. *Remote Sensing of Environment*, *22*(2), 209–233. https://doi.org/10.1016/0034-4257(87)90059-9

Choudhury, B. J., & Monteith, J. L. (1988). A four-layer model for the heat budget of homogeneous land surfaces. *Quarterly Journal of the Royal Meteorological Society*, *114*(480), 373–398. https://doi.org/10.1002/qj.49711448006

Cleugh, H. A., Leuning, R., Mu, G., & Running, S. W. (2007). Regional evaporation estimates from flux tower and MODIS satellite data. *Remote Sensing of Environment*, *106*(3), 285–304. https://doi.org/10.1016/j.rse.2006.07.007

Colaizzi, P. D., Agam, N., Tolk, J. A., Evett, S. R., Howell, T. A., Gowda, P., et al. (2014). Two source energy balance model to calculate E, T, and ET: Comparison of Priestly-Taylor and Penman-Monteith formulations and two time scaling methods. *Transactions of the ASABE*, *57*(2), 479–498.

Colaizzi, P.D., Agam, N., Tolk, J.A., Evett, S.R., Howell, T.A., Oshaughnessy, S.A., et al. (2013), The Penman-Monteith equation as a method to initialize canopy temperature in the two-source energy balance model and comparison to other methods. *ASA-CSSA-SSSA Annual Meeting Abstracts*. Session 195-10, p.123.

Colaizzi, P. D., Evett, S. R., Agam, N., Schwartz, R. C., & Kustas, W. P. (2016). Soil heat flux calculation for sunlit and shaded surfaces under row crops: 1. Model development and sensitivity analysis. *Agriculture and Forest Meterology.*, *216*, 115–128. https://doi.org/10.1016/j.agrformet.2015.10.010

Colaizzi, P. D., Evett, S. R., Howell, T. A., Gowda, P., O'Shaughnessy, S. A., Tolk, J. A., et al. (2012). Two source energy balance model: Refinements and lysimeter tests in the Southern High Plains. *Transactions of the ASABE*, *55*(2), 551–562. https://doi.org/10.13031/2013.41385

Colaizzi, P. D., Evett, S. R., Schwartz, R. C., Kustas, W. P., Cosh, M. H., & Mckee, L. G. (2016). Soil heat flux calculation for sunlit and shaded surfaces under row crops: 2. Model test. *Agricultural and Forest Meteorology*, *216*, 129–140. https://doi.org/10.1016/j.agrformet.2015.10.009

Colaizzi, P. D., Kustas, W. P., Anderson, M. C., Agam, N., Tolk, J. A., Evett, S. R., et al. (2012). Two-source energy balance model estimates of evapotranspiration using component and composite surface temperatures. *Advances in Water Resources*, *50*, 134–151. https://doi.org/10.1016/j.advwatres.2012.06.004

Decker, M., Or, D., Pitman, A., & Ukkola, A. (2017). New turbulent resistance parameterization for soil evaporation based on a pore-scale model: Impact on surface fluxes in CABLE. *Journal of Advances in Modeling Earth Systems*, *9*, 220–238. https://doi.org/10.1002/2016MS000832

Dinpashoh, Y. (2006). Study of reference crop evapotranspiration in I.R. of Iran. *Agricultural Water Management*, *84*(1-2), 123–129. https://doi.org/10.1016/j.agwat.2006.02.011

Elhag, M., Psilovikos, A., Manakos, I., & Perakis, K. (2011). Application of the SEBS water balance model in estimating daily evapotranspiration and evaporative fraction from remote sensing data over the Nile Delta. *Water Resources Management*, *25*(11), 2731–2742. https://doi.org/10.1007/s11269-011-9835-9

Fensholt, R., Langanke, T., Rasmussen, K., Reenberg, A., Prince, S. D., Tucker, C., et al. (2012). Greenness in semiarid areas across the globe 1981–2007—An Earth observing satellite based analysis of trends and drivers. *Remote Sensing of Environment*, *121*, 144–158. https://doi.org/10.1016/j.rse.2012.01.017

Fisher, J. B., Tu, K. P., & Baldocchi, D. D. (2008). Global estimates of the land-atmosphere water flux based on monthly AVHRR and ISLCP-II data, validated at 16 FLUXNET sites. *Remote Sensing of Environment*, *112*(3), 901–919. https://doi.org/10.1016/j.rse.2007.06.025

Foken, T. (2008). The energy balance closure problem: An overview. *Ecological Applications*, *18*(6), 1351–1367. https://doi.org/10.1890/06-0922.1

Frank, J. M., Massman, W. J., & Ewers, B. E. (2013). Underestimates of sensible heat flux due to vertical velocity measurement errors in non-orthogonal sonic anemometers. *Agricultural and Forest Meteorology*, *171*, 72–81.

Gao, F., Masek, J., Schwaller, M., & Hall, F. (2006). On the blending of the Landsat and MODIS surface reflectance: Predicting daily Landsat surface reflectance. *IEEE Transactions on Geoscience and Remote Sensing*, *44*(8), 2207–2218.

Garcia, M., Sandholt, I., Ceccato, P., Ridler, M., Mougin, E., Kergoat, L., et al. (2013). Actual evapotranspiration in drylands derived from in-situ and satellite data: Assessing biophysical constraints. *Remote Sensing of Environment*, *131*, 103–118. https://doi.org/10.1016/j.rse.2012.12.016

Gillies, J. A., Nickling, W. G., & King, J. (2002). Drag coefficient and plant form response to wind speed in three plant species: Buring bush (Euonymus alatus), Colorada blue spruce (Pricea pungens glauca), and Fountian grass (Pennisetum setaceum). *Journal of Geophysical Research*, *107*(D24), 4760. https://doi.org/10.1029/2001JD001259

Gokmen, M., Vekerdy, Z., Verhoef, A., Verhoef, A., Batelaan, O., & Van Der Tol, C. (2012). Integration of soil moisture in SEBS for improving evapotranspiration estimation under water stress conditions. *Remote Sensing of Environment*, *121*, 261–274. https://doi.org/10.1016/j.rse.2012.02.003

Gutman, G., & Ignatov, A. (1998). The derivation of the green vegetation fraction from NOAA/AVHRR data for use in numerical weather prediction models. *International Journal of Remote Sensing*, *19*(8), 1533–1543. https://doi.org/10.1080/014311698215333

Haghighi, E., & Kirchner, J. W. (2017). Near-surface turbulence as a missing link in modeling evaportranspiration-soil moisture relationships. *Water Resources Research*, *53*, 5320–5344. https://doi.org/10.1002/2016WR020111

Haghighi, E., & Or, D. (2013). Evaporation from porous surfaces into turbulent airflows: Coupling eddy characteristics with pore scale vapour diffusion. *Water Resources Research*, *49*, 8432–8442. https://doi.org/10.1002/2012WR013324
Haghighi, E., & Or, D. (2015a). Linking evaporative fluxes from bare soil across surface viscous sublayer with the Monin-Obukhov atmosphere flux-profile estimates. *Journal of Hydrology*, *525*, 684–693. https://doi.org/10.1016/j.jhydrol.2015.04.019
Haghighi, E., & Or, D. (2015b). Interactions of bluff-body obstacles with turbulent airflows affecting evaporative fluxes from porous surface. *Journal of Hydrology*, *530*, 103–116. https://doi.org/10.1016/j.jhydrol.2015.09.048
Haghighi, E., & Or, D. (2015c). Thermal signatures of turbulent airflows interacting with evaporating thin porous surfaces. *International Journal of Heat and Mass Transfer*, *87*, 429–446. https://doi.org/10.1016/j.ijheatmasstransfer.2015.04.026
Haghighi, E., & Or, D. (2015d). Turbulence-induced thermal signatures over evaporating bare soil surfaces. *Geophysical Research Letters*, *42*, 5325–5336. https://doi.org/10.1002/2015GL064354
Haghighi, E., Shahraeeni, E., Lehmann, P., & Or, D. (2013). Evaporation rates across a convective air boundary layer are dominated by diffusion. *Water Resources Research*, *49*, 1602–1610. https://doi.org/10.1002/wrcr.20166
Herman, J., & Usher, W. (2017). Salib: An open-source python library for sensitivity analysis. *Journal of Open Source Software*, (9), 97.
Huang, C. L., Li, Y., Gu, J., Lu, L., & Li, X. (2015). Improving estimation of evapotranspiration under water-limited conditions based on SEBS and MODIS data in arid regions. *Remote Sensing*, *7*(12), 16,795–16,814. https://doi.org/10.3390/rs71215854
Jacobs, A. F. G., Verhoef, A., & Bruin, H. A. R. D. (1996). Sensible heat flux from sparse vegetation estimated using Nusselt numbers. *Physics and Chemistry of the Earth*, *21*(3), 107–110. https://doi.org/10.1016/S0079-1946(97)85569-3
Kalma, J. D., McVicar, T. R., & McCabe, M. F. (2008). Estimating land surface evaporation: A review of methods using remotely sensed surface temperature data. *Surveys in Geophysics*, *29*(4–5), 421–469. https://doi.org/10.1007/s10712-008-9037-z
Kochendorfer, J., Meyers, T. P., Frank, J., Massman, W. J., & Heuer, M. W. (2012). How well can we measure the vertical wind speed? Implications for fluxes of energy and mass. *Boundary-Layer Meteorology*, *145*(2), 383–398. https://doi.org/10.1007/s10546-012-9738-1
Kondo, J., & Ishida, S. (1997). Sensible heat flux from the Earth's surface under natural convective conditions. *Journal of the Atmospheric Sciences*, *54*(4), 498–509. https://doi.org/10.1175/1520-0469(1997)054<0498:SHFFTE>2.0.CO;2
Kustas, W. P., & Anderson, M. C. (2009). Advances in thermal infrared remote sensing for land surface modeling. *Agricultural and Forest Meteorology*, *149*(12), 2071–2081. https://doi.org/10.1016/j.agrformet.2009.05.016
Kustas, W. P., & Daughtry, C. S. T. (1990). Estimation of the soil heat flux/net radiation ratio from spectral data. *Agricultural and Forest Meteorology*, *49*(3), 205–223. https://doi.org/10.1016/0168-1923(90)90033-3
Kustas, W. P., Humes, K. S., Norman, J. M., & Moran, M. S. (1996). Single- and dual-source modeling of surface energy fluxes with radiometric surface temperature. *Journal of Applied Meteorology*, *35*(1), 110–121. https://doi.org/10.1175/1520-0450(1996)035<0110:SADSMO>2.0.CO;2
Kustas, W. P., Nieto, H., Morillas, L., Anderson, M. C., Alfieri, J. G., Hipps, L. E., et al. (2016). Revisiting the paper "using radiometric surface temperature for surface energy flux estimation in Mediterranean drylands from a two-source perspective". *Remote Sensing of Environment*, *184*, 645–653. https://doi.org/10.1016/j.rse.2016.07.024
Kustas, W. P., & Norman, J. M. (1999). Evaluation of soil and vegetation heat flux predictions using a simple two-source model with radiometric temperatures for partial canopy cover. *Agricultural and Forest Meteorology*, *94*(1), 13–29. https://doi.org/10.1016/S0168-1923(99)00005-2
Kustas, W. P., & Norman, J. M. (2000). A two-source energy balance approach using directional radiometric temperature observations for sparse canopy covered surfaces. *Agronomy Journal*, *92*(5), 847–854. https://doi.org/10.2134/agronj2000.925847x
Kustas, W. P., Prueger, J. H., Hatfield, J. L., Ramalingam, K., & Hipps, L. E. (2000). Variability in soil heat flux from a mesquite dune site. *Agricultural and Forest Meteorology*, *103*(3), 249–264. https://doi.org/10.1016/S0168-1923(00)00131-3
Leuning, R., van Gorsel, E., Massman, W. J., & Issac, P. R. (2012). Reflections on the surface energy imbalance problem. *Agricultural and Forest Meteorology*, *156*, 65–74. https://doi.org/10.1016/j.agrformet.2011.12.002
Li, F., Kustas, W. P., Anderson, M. C., Prueger, J. H., & Scott, R. L. (2008). Effect of remote sensing spatial resolution on interpreting tower-based flux observations. *Remote Sensing of Environment*, *112*(2), 337–349. https://doi.org/10.1016/j.rse.2006.11.032
Li, F., Kustas, W. P., Prueger, J. H., Neale, C. M., & Jackson, T. J. (2005). Utility of remote sensing–based two-source energy balance model under low-and high-vegetation cover conditions. *Journal of Hydrometeorology*, *6*(6), 878–891. https://doi.org/10.1175/JHM464.1
Li, X., Cheng, G., Liu, S., Xiao, Q., Ma, M., Jin, R., et al. (2013). Heihe watershed allied telemetry experimental research (HiWATER): Scientific objectives and experimental design. *Bulletin of the American Meteorological Society*, *94*(8), 1145–1160. https://doi.org/10.1175/BAMS-D-12-00154.1
Li, Y., Huang, C., Hou, J., Gu, J., Zhu, G., & Li, X. (2017). Mapping daily evapotranspiration based on spatiotemporal fusion of ASTER and MODIS images over irrigated agricultural areas in the Heihe River Basin, Northwest China. *Agricultural and Forest Meteorology*, *244*, 82–97.
Li, Y., Kustas, W. P., Huang, C., Kool, D., & Haghighi, E. (2018). Evaluation of soil resistance formulations for estimates of sensible heat flux in a desert vineyard. *Agricultural and Forest Meteorology*, *260-261*, 255–261. https://doi.org/10.1016/j.agrformet.2018.06.019
Liang, S. L. (2004). *Quantitative remote sensing of land surface* (pp. 345–348). Hoboken, NJ: Wiley.
Liebethal, C., Huwe, B., & Foken, T. (2005). Sensitivity analysis for two ground heat flux calculation approaches. *Agricultural and Forest Meteorology*, *132*(3-4), 253–262. https://doi.org/10.1016/j.agrformet.2005.08.001
Mayaud, J. R., Wiggs, G. F. S., & Bailey, R. M. (2016). Characterizing turbulent wind flow around dryland vegetation. *Earth Surface Processes and Landforms*, *41*(10), 1421–1436. https://doi.org/10.1002/esp.3934
Moran, M. S. (2004). Thermal infrared measurement as an indicator of plant ecosystem health. *Thermal remote sensing in land surface processes*, *257-282*. https://doi.org/10.1201/9780203502174-c9
Morillas, L., García, M., Nieto, H., Villagarcia, L., Sandholt, I., Gonzalez-Dugo, M. P., et al. (2013). Using radiometric surface temperature for surface energy flux estimation in Mediterranean drylands from a two-source perspective. *Remote Sensing of Environment*, *136*, 234–246. https://doi.org/10.1016/j.rse.2013.05.010
Norman, J. M., Kustas, W. P., & Humes, K. S. (1995). Source approach for estimating soil and vegetation energy fluxes in observations of directional radiometric surface temperature. *Agricultural and Forest Meteorology*, *77*(3-4), 263–293. https://doi.org/10.1016/0168-1923(95)02265-Y
Ochsner, T. E., Sauer, T. J., & Horton, R. (2006). Field tests of the soil heat flux plate method and some alternatives. *Agronomy Journal*, *98*(4), 1005–1014. https://doi.org/10.2134/agronj2005.0249
Palau-Salvador, G., Stoesser, T., Fröhlich, J., Kappler, M., & Rodi, W. (2010). Large eddy simulations and experiments of flow around finite-height cylinders. *Flow, Turbulence and Combustion*, *84*(2), 239–275. https://doi.org/10.1007/s10494-009-9232-0
Raupach, M. R. (1992). Drag and drag partition on rough surfaces. *Boundary-Layer Meteorology*, *60*(4), 375–395. https://doi.org/10.1007/BF00155203

Saltelli, A., Tarantola, S., & Chan, P. S. (1999). A quantitative model-independent method for global sensitivity analysis of model output. *Technometrics*, *41*(1), 39–56. https://doi.org/10.1080/00401706.1999.10485594

Sauer, T. J., Norman, J. M., Tannar, C. B., & Wilson, T. B. (1995). Measurement of heat and vapour transfer coefficients at the soil surface beneath a maize canopy using source plates. *Agricultural and Forest Meteorology*, *75*(1-3), 161–189. https://doi.org/10.1016/0168-1923(94)02209-3

Scanlon, T. M., & Kustas, W. P. (2012). Partitioning evapotranspiration using an eddy covariance-based technique: Improved assessment of soil moisture and land–atmosphere exchange dynamics. *Vadose Zone Journal*, *11*(3). https://doi.org/10.2136/vzj2012.0025

Scott, R. L. (2010). Using watershed water balance to evaluate the accuracy of eddy covariance evaporation measurements for three semiarid ecosystems. *Agricultural and Forest Meteorology*, *150*(2), 219–225. https://doi.org/10.1016/j.agrformet.2009.11.002

Scott, R. L., Biederman, J. A., Hamerlynck, E. P., & Barron-Gafford, G. A. (2015). The carbon balance pivot point of southwestern U.S. semiarid ecosystems: Insights from the 21st century drought. *Journal of Geophysical Research: Biogeosciences*, *120*, 2612–2624. https://doi.org/10.1002/2015JG003181

Shao, Y. P., & Yang, Y. (2008). A theory for drag partition over rough surface. *Journal of Geophysical Research*, *113*, F02S05. https://doi.org/10.1029/2007JF000791

Song, L. S., Kustas, W. P., Liu, S., Colaizzi, P. D., Nieto, H., Xu, Z., et al. (2016). Applications of a thermal-based two-source energy balance model using Priestley-Taylor approach for surface temperature partitioning under advective conditions. *Journal of Hydrology*, *540*, 574–587. https://doi.org/10.1016/j.jhydrol.2016.06.034

Song, L. S., Liu, S. M., Kustas, W. P., Zhou, J., Xu, Z. W., Xia, T., & Li, M. S. (2016). Application of remote sensing-based two-source energy balance model for mapping field surface fluxes with composite and component surface temperatures. *Agricultural and Forest Meteorology*, *230–231*, 8–19.

Stewart, J. B., Kustas, W. P., Humes, K. S., Nichols, W. D., Moran, M. S., & de Bruin, H. A. R. (1994). Sensible heat flux-radiometric surface temperature relationship for 8 semi-arid areas. *Journal of Applied Meteorology*, *33*(9), 1110–1117. https://doi.org/10.1175/1520-0450(1994)033<1110:SHFRST>2.0.CO;2

Talsma, C. J., Good, S. P., Jimenez, C., Martens, B., Fisher, J. B., Miralles, D. G., et al. (2018). Partitioning of evapotranspiration in remote sensing-based models. *Agricultural and Forest Meteorology*, *260-261*, 131–143. https://doi.org/10.1016/j.agrformet.2018.05.010

Tang, R., Li, Z. L., Jia, Y., Li, C., Sun, X., Kustas, W. P., & Anderson, M. C. (2011). An intercomparison of three remote sensing-based energy balance models using Large Aperture Scintillometer measurements over a wheat-corn production region. *Remote Sensing of Environment*, *115*(12), 3187–3202. https://doi.org/10.1016/j.rse.2011.07.004

Timmermans, W. J., Kustas, W. P., Anderson, M. C., & French, A. N. (2007). An intercomparison of the surface energy balance algorithm for land (SEBAL) and the two-source energy balance (TSEB) modeling schemes. *Remote Sensing of Environment*, *108*(4), 369–384. https://doi.org/10.1016/j.rse.2006.11.028

Van der Kwast, J., Timmermans, W., Gieske, A., Su, Z., Olioso, A., Jia, L., et al. (2009). Evaluation of the surface energy balance system (SEBS) applied to ASTER imagery with flux-measurements at the SPARC 2004 site (Barrax Spain). *Hydrology and Earth System Sciences Discussions*, *6*(1), 1165–1196. https://doi.org/10.5194/hessd-6-1165-2009

Wang, J., Zhuang, J., Wang, W., Liu, S., & Xu, Z. (2015). Assessment of uncertainties in eddy covariance flux measurement based on intensive flux matrix of HiWATER-MUSOEXE. *IEEE Geoscience and Remote Sensing Letters*, *12*(2), 259–263. https://doi.org/10.1109/LGRS.2014.2334703

Wang, K., & Dickinson, R. E. (2012). A review of global terrestrial evapotranspiration: Observation, modeling, climatology, and climatic variability. *Reviews of Geophysics*, *50*, RG2005. https://doi.org/10.1029/2011RG000373

Wilcox, B. P., Breshears, D. D., & Seyfried, M. S. (2003). Water balance on rangelands. In B. A. Stewart, & T. A. Howell (Eds.), *Encyclopedia of Water Science*, (pp. 791–794). New York: Marcel Dekker, Inc.

Xu, Z., Liu, S., Li, X., Shi, S., Wang, J., Zhu, Z., et al. (2013). Intercomparison of surface energy flux measurement systems used during the HiWATER-MUSOEXE. *Journal of Geophysical Research: Atmospheres*, *118*, 13,140–13,157. https://doi.org/10.1002/2013JD020260

Xu, Z., Ma, Y., Liu, S., Shi, W., & Wang, J. (2017). Assessment of the energy balance closure under Advective conditions and its impact using remote sensing data. *Journal of Applied Meteorology and Climatology*, *56*(1), 127–140. https://doi.org/10.1175/JAMC-D-16-0096.1

Zhan, X., Kustas, W. P., & Humes, K. S. (1996). An intercomparison study on models of sensible heat flux over partial canopy surfaces with remotely sensed surface temperature. *Remote Sensing of Environment*, *58*(3), 242–256. https://doi.org/10.1016/S0034-4257(96)00049-1